JOURNAL OF APPLIED PHYSICS **113**, 124302 (2013)

Environmental decoherence stabilizes quantum-dot cellular automata

Enrique P. Blair and Craig S. Lent[a)]
Department of Electrical Engineering, University of Notre Dame, Notre Dame, Indiana 46556, USA

(Received 26 November 2012; accepted 8 March 2013; published online 27 March 2013)

We consider the effects of interaction with the environment on decoherence in quantum-dot cellular automata (QCA). We model the environment as a Coulombically interacting random assembly of quantum double-dots. The time evolution of our model system + environment is unitary and maintains one coherent state. We explicitly calculate the reduced density operators for the system and for the environment from the full coherent state. From the reduced density matrix of the system, we calculate the coherence vector and the Von Neumann entropy. The entanglement of system and environmental degrees of freedom lead to decoherence, which drives the system into the Zurek pointer states. The quantum information lost by the system, quantified by the entropy, is present in the quantum mutual information between the system and the environment. We explore the competition between environmental decoherence and system dynamics. For even a modest environmental interaction, the pointer states are the QCA information-bearing degrees of freedom, so that environmental decoherence, while destructive of quantum information, tends to stabilize QCA bit information. © *2013 American Institute of Physics*. [http://dx.doi.org/10.1063/1.4796186]

I. INTRODUCTION

A search is underway for a successor technology to the solid-state transistor for logic applications.[1] Field-effect transistors, which are basically voltage-controlled current switches, have significant limitations when critical dimensions are scaled down to a few nanometers.[2] A successful alternative would need to represent binary information, provide an efficient switching mechanism between states, operate at device densities down to the single-molecule scale, and dissipate very little heat during a binary state transition.

One promising approach is quantum-dot cellular automata (QCA), in which binary information is represented by the configuration of charge among a set of quantum dots. The simplest QCA cell is a double-dot with a single mobile charge whose location on one dot or the other represents a binary 1 or 0.[3] In this case, a quantum dot can be considered any potential well that can localize electrons or holes. Hopping from dot to dot is through quantum mechanical tunneling. The dots are arranged to form QCA cells; no current flows from cell to cell. The intercellular coupling is through the Coulomb interaction. Clocked control of QCA cells is made possible by the effect of locally applied electric fields, which can switch molecules between active information-bearing states and a null state.[4] If QCA cells can be synthesized and placed on a surface in specific patterns, general-purpose computing is possible. Circuit architectures that can efficiently exploit QCA capabilities are an active area of research.[5]

Several ways of implementing the QCA paradigm are being explored. QCA devices have been fabricated in semiconductor depletion dots in GaAs.[6] QCA cells with dots formed by carefully implanted donors in Si have also been demonstrated.[7] Wolkow *et al.*[8] have used dots that are single dangling bonds on a Si surface to form a QCA cell of single-nanometer size operating at room temperature. Mixed-valence molecules designed to have mobile electrons, which can tunnel from one site to another within the molecule have been synthesized and shown to exhibit the requisite bistable saturation. Fairly complex QCA circuits, including logic gates and shift registers, have been demonstrated using dots formed from isolated Al islands in the Coulomb blockade regime, albeit at cryogenic temperatures. Power gain has been demonstrated in these systems. A magnetic version of QCA, in which magnetic dipoles replace electrical dipoles, has also shown promise.[9]

QCA operation is quantum mechanical in that switching is by quantum tunneling from dot to dot. Barriers between dots must be high enough for mobile electrons to localize, i.e., the expectation value of the number operator on a particular dot is very nearly integer. The bit information in QCA is, however, encoded in the classical degree of freedom corresponding to the dipole or quadrupole moment of the charge distribution. In fact, it is only the *sign* of the moment that represents the bit. (There have been proposals for using the continuous value to enable analog QCA operation.) QCA is not quantum computing and does not use qubits to encode information.

For molecular-scale implementations, including both mixed-valence molecules and dangling surface bonds, however, it may be possible that quantum coherence across one or several cells could be maintained, though that such coherence could survive at room temperature is not clear. The interesting question of whether phase coherence could in fact pose problems for QCA operation has been recently raised by Taucer *et al.*[10]

The issue of a possibly destructive result of quantum phase coherence focuses attention on a fundamental fact about any physical device that contains local memory. Consider a physical system which stores and processes at least one binary bit. Suppose, the value of the bit was written to it by an input mechanism at sometime in the past, but the input system no longer interacts with the memory/computing

[a)]lent@nd.edu

system after the writing is complete. At any subsequent time t, whether the system is in the state representing a binary 1 or 0 must not be determined by the just the spatial boundary conditions and the current Hamiltonian $\hat{H}$. If it were, it could not hold a value that depends on the input. The physical state of a memory device cannot be determined simply by its surroundings: it must be determined also by its history. The state encoding a stored bit cannot be an eigenstate of $\hat{H}$. Since, from a physical point of view the bit could equally well be in a 1 or a 0 state, the physical system must be in a long-lived metastable state rather than a stationary state of the Hamiltonian. As a consequence, if quantum coherence is maintained indefinitely, the system should tunnel back and forth between the 1 state and the 0 state, executing coherent Rabi oscillations. (We are assuming here that there is no internal bias that prefers one state over another energetically.) This consideration applies not just to QCA, but to any system representing information by the physical system state. The stationary states of the memory system are the symmetric and antisymmetric superpositions of the 1 and 0 states. In most systems, including CMOS and QCA, the energy splitting between these two Hamiltonian eigenstates is extremely small because there is a large effective barrier between the 1 and 0 states. This normally provides a very substantial kinetic barrier between the two information-bearing states, and coherent oscillations—if they were observable—would have a very long period. Decoherence due to environmental interactions would destroy these Rabi oscillations before they ever got started; but, clearly this becomes a quantitative question which could be examined in particular systems.

Here, we address the issue of unwanted coherent oscillations and environmental decoherence as part of a larger study of the interaction between QCA systems and the environment. Our approach is to construct a simple model that contains the minimal elements necessary to explore the relationship between the coherent system dynamics and the entanglement with the environment that causes decoherence. We consider first a single QCA double-dot with an environment comprised of randomly oriented neutral double-dots at zero temperature. This is by design a minimally perturbing environment. Section II defines this model. Dynamics are calculated both numerically and analytically by direct computation of the unitary time evolution of the combined system + environment. Measures of coherence and quantum information flow are also employed. Section III considers the dynamics in the absence of an environment. Section IV examines the dynamics, when the environment completely dominates the internal system dynamics. The general case, when both internal dynamics and environmental decoherence compete is explored in Section V. The impact of a larger system on the fragility of quantum coherence is addressed in Section IV by using a pair of double-dot systems. A discussion of the results follows.

We find particularly helpful in understanding this behavior the contributions of Zurek and coworkers on the general theory of decoherence and pointer states.[11] In understanding, the nature of the entropy as a measure of missing information, the work of Ben-Naim is particularly clarifying.[12]

II. MODEL SYSTEM PLUS ENVIRONMENT

A. System

We consider a system which consists of a two-dot QCA cell with one mobile electron and interdot distance a. We take $a = 0.7\,\text{nm}$, corresponding to the scale of QCA molecules. This system cell in isolation is described using a two-state basis.

$$|\psi^{\mathcal{S}}\rangle = c_0|0^{\mathcal{S}}\rangle + c_1|1^{\mathcal{S}}\rangle. \tag{1}$$

Here, $|0^{\mathcal{S}}\rangle$ and $|1^{\mathcal{S}}\rangle$ represent the system states with the electron completely localized on one or the other dot, encoding a binary "0" or "1." These completely localized states are the computational basis states for the system.

The Hamiltonian for the isolated system cell is

$$\hat{H}^0_{\mathcal{S}} = -\gamma[|1^{\mathcal{S}}\rangle\langle 0^{\mathcal{S}}| + |0^{\mathcal{S}}\rangle\langle 1^{\mathcal{S}}|]. \tag{2}$$

We assume that in addition to the mobile electronic charge, there are fixed neutralizing charges of $+e/2$ on each of the two dots. In the actual molecule, this neutralizing charge is either a donor center[13] or a counterion.[14,15] The model reflects the reality that molecular QCA cells have a nonzero dipole moment, but no net charge.

By design, the system Hamiltonian has no diagonal terms that break the symmetry between the $|0^{\mathcal{S}}\rangle$ and $|1^{\mathcal{S}}\rangle$ states, i.e., there is no preferred state. In QCA circuits, the presence of a neighboring cell breaks this symmetry, providing the coupling between devices that makes logical operations possible.

B. Environment

We construct here a very simple model of the environment using many two-dot cells to mimic degrees of freedom in the environment that couple Coulombically to the system cell. The intent is to make a simple, very minimal model of the environment as a set of N neutral two-dot cells. The environment cells are labeled with an integer $k \in [1, 2, ..., N]$; the index $k = 0$ will denote the system cell. We assume that the environment cells have no tunneling between the two dots ($\gamma_{\mathcal{E}} = 0$), so the Hamiltonian for the kth environment cell in isolation is $\hat{H}^{\mathcal{E}}_k = 0$. This does not account for the Coulomb interaction between environment cells, which will be included later. We emphasize that these cells are not meant to describe other QCA cells in the circuit, but rather represent a very minimal environment, which is neutral and non-switching.

The state vector for kth environment cell in isolation is given by

$$|\psi^{\mathcal{E}}_k\rangle = c^k_0|0^{\mathcal{E}}_k\rangle + c^k_1|1^{\mathcal{E}}_k\rangle. \tag{3}$$

As with the system cell, a fixed neutralizing charge of $+e/2$ is present on each of the dots.

It will be helpful to label the computational basis states $|0\rangle$ and $|1\rangle$ of the system and each environment cell with an index $m = 0$ or 1 for the two states.

For the system cell

$$|\alpha_0^{\mathcal{S}}\rangle = |0^{\mathcal{S}}\rangle, \quad |\alpha_1^{\mathcal{S}}\rangle = |1^{\mathcal{S}}\rangle. \tag{4}$$

For the kth environment cell

$$|\alpha_{k,0}^{\mathcal{E}}\rangle = |0_k^{\mathcal{E}}\rangle, \quad |\alpha_{k,1}^{\mathcal{E}}\rangle = |1_k^{\mathcal{E}}\rangle. \tag{5}$$

C. Geometry

Within our model, we establish a geometry for the system and environment which provides control over the system-environment interaction. In each case, the system is placed at the origin, and the N cells providing the environment are placed at random sites on the surface of a sphere of radius R centered on the system with random orientations. The environment population N and radius R provide control over the strength of the system-environment interaction, and the random orientations of the environmental cells add non-uniformity in this interaction.

Figure 1 shows one such geometry for a eight-cell environment ($N=8$). Each pair of small, colored balls connected by a black stick represents a molecule. Each colored ball represents a quantum dot, and its color indicates the net charge locally present: red indicates negative charge (the dot is occupied by an electron), green indicates positive charge (no electron is present), and grey is charge-neutral (the molecule has zero polarization, with an expectation value of one-half for finding the electron localized on either dot). The connecting black stick is the tunneling path for intramolecular charge tunneling. Figure 1 shows the system polarized in one of the computational basis states with all the environment cells in depolarized states.

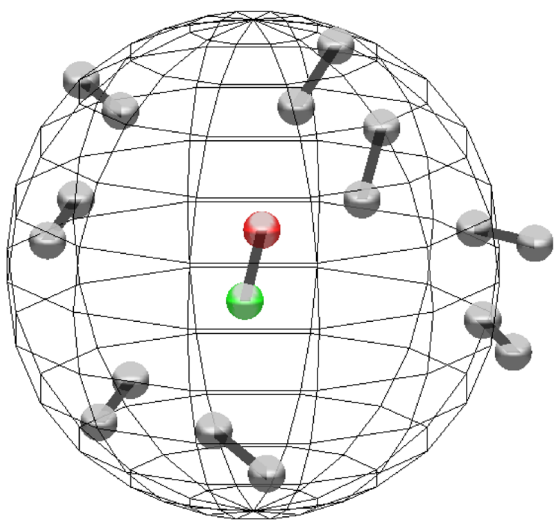

FIG. 1. A schematic view of the model geometry. The system cell, a coupled pair of quantum dots, is surrounded by the environment, represented by quantum double dots. The small spheres represent quantum dots, and the black bars connecting them represent intra-molecular interdot tunneling paths. N environmental cells are randomly located on a sphere of radius R, with random orientations. For this minimal representation of the environment, the environmental cells are always neutral, with equal probabilities of electron occupancy on each dot.

D. Entanglement of the system with the environment

The system-plus-environment is represented by a single pure state vector, which is in the space spanned by the direct products of the states of the system cell and all environmental cells.

$$|\psi(t)\rangle = \sum_{\substack{m_0=0\\ m_1=0\\ \vdots\\ m_N=0}}^{1} c_{m_0,m_1,\ldots,m_N}(t)|\alpha_{m_0}^{\mathcal{S}}\rangle|\alpha_{1,m_1}^{\mathcal{E}}\rangle|\alpha_{2,m_2}^{\mathcal{E}}\rangle\ldots|\alpha_{N,m_N}^{\mathcal{E}}\rangle. \tag{6}$$

Each basis state configuration of the environment in the direct product space of Eq. (6) is specified by a set N integers $m_k \in \{0,1\}$, which we treat as an N-dimensional vector.

$$\vec{m} \equiv [m_1, m_2, \ldots, m_N]. \tag{7}$$

There are $N_{\mathcal{E}} = 2^N$ such vectors in the basis set, $[\vec{m}_1, \vec{m}_2, \vec{m}_3, \ldots, \vec{m}_{N_{\mathcal{E}}}]$, each representing a specific configuration of $\mathcal{E}$.

$$\begin{aligned} \vec{m}_1 &= [0,0,0,\ldots,0],\\ \vec{m}_2 &= [1,0,0,\ldots,0],\\ \vec{m}_3 &= [0,1,0,\ldots,0],\\ \vec{m}_4 &= [1,1,0,\ldots,0],\\ &\vdots \qquad\qquad \vdots\\ \vec{m}_{N_{\mathcal{E}}} &= [1,1,1,\ldots,1]. \end{aligned} \tag{8}$$

Equation (6) can be rewritten as a sum over the system degrees of freedom and the environment degrees of freedom.

$$|\psi(t)\rangle = \sum_{m_0=0}^{1}\sum_{p=1}^{N_{\mathcal{E}}} c_{m_0,\vec{m}_p}(t)|\alpha_{m_0}^{\mathcal{S}};\alpha_{\vec{m}_p}^{\mathcal{E}}\rangle. \tag{9}$$

E. Dynamics

The Hamiltonian of the system + environment can be written as the sum of the system Hamiltonian, the environment Hamiltonian, and the interaction between the system and the environment.

$$\hat{H} = \hat{H}_{\mathcal{S}} + \hat{H}_{\mathcal{E}} + \hat{H}_{\mathcal{SE}}, \tag{10}$$

where $\hat{H}_{\mathcal{S}}$ is the isolated system Hamiltonian of Eq. (2). The Hamiltonian for the environment $\hat{H}_{\mathcal{E}}$ includes all the Coulomb interactions between environment cells and $\hat{H}_{\mathcal{SE}}$ represents the Coulomb interactions between the system cell and the cells in the environment. The complete Hamiltonian $\hat{H}$ can be represented by a $2^{N+1} \times 2^{N+1}$ matrix.

The Hamiltonian for the environment $\hat{H}_{\mathcal{E}}$, and the system-environment interaction $\hat{H}_{\mathcal{SE}}$, can each be expressed in terms of the Coulomb potential energy for two interacting cells.

Let $U_{m_j,m_k}^{j,k}$ be the electrostatic potential energy between the jth cell in state m_j (0 or 1) and the kth cell in state m_k (0 or 1). This energy is given by

$$U^{j,k}_{m_j,m_k} = \frac{P(m_j)P(m_k)e^2}{16\pi\epsilon_o}\left[\frac{1}{r^{j,k}_{0,0}} - \frac{1}{r^{j,k}_{0,1}} - \frac{1}{r^{j,k}_{1,0}} + \frac{1}{r^{j,k}_{1,1}}\right], \quad (11)$$

where e is the fundamental charge, ϵ_o is the permittivity of free space, $r^{j,k}_{m_j,m_k}$ is the distance between dot m_j in cell j and dot m_k in cell k, and $P(m)$ is the polarization of a cell in state m. $P(1) = +1$ and $P(0) = -1$.

Because each cell in the environment has no interdot tunneling, the Hamiltonian for the environment $\hat{H}_{\mathcal{E}}$ is diagonal in this basis and is given by Eq. (9).

$$\hat{H}_{\mathcal{E}} = \left[\sum_{p=1}^{N_{\mathcal{E}}} |\alpha^{\mathcal{E}}_{\vec{m}_p}\rangle E^{\mathcal{E}}_{\vec{m}_p} \langle\alpha^{\mathcal{E}}_{\vec{m}_p}|\right] \otimes \hat{I}_{\mathcal{S}}. \quad (12)$$

The diagonal elements of $\hat{H}_{\mathcal{E}}$ are the potential energies associated with each basis state, which can be expressed as a sum over all the pairwise interactions between environment cells.

$$E^{\mathcal{E}}_{\vec{m}_p} = \frac{1}{2}\sum_{\substack{j,k=1 \\ j\neq k}}^{N_{\mathcal{E}}} U^{j,k}_{m^j_p,m^k_p}. \quad (13)$$

Here, $m^k_p = [\vec{m}_p]_k$, the state of the kth cell in environment configuration p.

The system-environment interaction Hamiltonian $\hat{H}_{\mathcal{SE}}$ is also diagonal in the site basis.

$$\hat{H}_{\mathcal{SE}} = \sum_{p=1}^{N_{\mathcal{E}}}\sum_{m_0=0}^{1} |\alpha^{\mathcal{S}}_{m_0}; \Psi^{\mathcal{E}}_{\vec{m}_p}\rangle E^{\mathcal{SE}}_{m_0;\vec{m}_p} \langle\alpha^{\mathcal{S}}_{m_0}; \Psi^{\mathcal{E}}_{\vec{m}_p}|. \quad (14)$$

Here, $|\Psi^{\mathcal{E}}_{\vec{m}_p}\rangle$ is a product state of environmental cell computational basis states as specified by $\vec{m}_p$

$$|\Psi^{\mathcal{E}}_{\vec{m}_p}\rangle = |\alpha^{\mathcal{E}}_{1,m_1}\rangle|\alpha^{\mathcal{E}}_{2,m_2}\rangle\cdots|\alpha^{\mathcal{E}}_{N,m_N}\rangle. \quad (15)$$

The energy $E^{\mathcal{SE}}_{m_0;\vec{m}_p}$ is the Coulomb potential energy of the state with the environment $\mathcal{E}$ in the state specified by $\vec{m}_p$ and the system $\mathcal{S}$ in the state specified by bit m_0.

$$E^{\mathcal{SE}}_{m_0;\vec{m}_p} = \sum_{k=1}^{N} U^{0,k}_{m_0,m_k}. \quad (16)$$

We define the bit flip energy $E^{\text{flip}}_{\vec{m}_p}$ for each configuration of the environment.

$$E^{\text{flip}}_{\vec{m}_p} \equiv E^{\mathcal{SE}}_{1;\vec{m}_p} - E^{\mathcal{SE}}_{0;\vec{m}_p}. \quad (17)$$

This is the energy required to flip the system cell state from 0 to 1, for each environmental configuration $\vec{m}_p$.

The Hamiltonian for the two-dot system is embedded in the larger Hilbert space, which includes the environmental degrees of freedom.

$$\hat{H}_{\mathcal{S}} = \hat{1}_{\mathcal{E}} \otimes \hat{H}^0_{\mathcal{S}} = \hat{1}_{\mathcal{E}} \otimes [-\gamma\hat{\lambda}^{\mathcal{S}}_1]. \quad (18)$$

F. Density operator and time evolution

The density operator for the whole system + environment is given by

$$\hat{\rho}(t) = |\psi(t)\rangle\langle\psi(t)|. \quad (19)$$

The system + environment is one coherent quantum system that evolves under the quantum Liouville equation.

$$\hat{\rho}(t) = e^{-\frac{i}{\hbar}\hat{H}t}\hat{\rho}(0)e^{+\frac{i}{\hbar}\hat{H}t}. \quad (20)$$

The Hamiltonian, here is the complete Hamiltonian of Eq. (10), the sum of $\hat{H}_{\mathcal{E}}$ from Eq. (12), $\hat{H}_{\mathcal{SE}}$ from Eq. (14), and $\hat{H}_{\mathcal{S}}$ from Eq. (18).

An initial density matrix is chosen for the system cell $\hat{\rho}_{\mathcal{S}}(0)$ and the density matrix $\hat{\rho}_k(0)$ for each of the environment cells. The environment density matrix is the direct product of the density matrices for each cell, and the complete density matrix is the direct product of the environment and system density matrices.

$$\hat{\rho}_{\mathcal{E}}(0) = \hat{\rho}_1(t) \otimes \hat{\rho}_2(t)\ldots \otimes \hat{\rho}_N(t), \quad (21)$$

$$\hat{\rho}(0) = \hat{\rho}_{\mathcal{E}}(0) \otimes \hat{\rho}_{\mathcal{S}}(0). \quad (22)$$

Note that only the initial state is a direct product state—the time evolution given by Eq. (20) quickly mixes product states together. In the calculations we report here, we always take the initial state to be a direct product of pure states for the system and environment, but the evolved system is always in a superposition of product states, as in Eq. (9).

The reduced density matrix for the system is calculated by directly summing over the 2^N environmental degrees of freedom.

$$\hat{\rho}^r_{\mathcal{S}}(t) = \underset{m_1,m_2,\ldots,m_N}{\text{Tr}} \hat{\rho}(t) = \underset{\vec{m}}{\text{Tr}}\ \hat{\rho}(t). \quad (23)$$

The reduced density matrix for the environment is calculated by summing over the system cell's degrees of freedom.

$$\hat{\rho}^r_{\mathcal{E}}(t) = \underset{m_0}{\text{Tr}}\ \hat{\rho}(t). \quad (24)$$

In a similar way, the reduced density matrix for any subset of the environment, or indeed any combination of cells, can also be calculated by summing over the unwanted, or unknown, degrees of freedom.

The reduced density matrix for the system cell must be Hermitian and have unit trace. As a consequence it can be written as a linear combination of the identity and the generators of SU(2), $\hat{\lambda}_1, \hat{\lambda}_2$, and $\hat{\lambda}_3$ (the Pauli matrices).[16]

$$\begin{aligned}\hat{\rho}^r_{\mathcal{S}}(t) &= \frac{1}{2}\{\hat{1} + \lambda_1\hat{\lambda}_1 + \lambda_2\hat{\lambda}_2 + \lambda_3\hat{\lambda}_3\}, \\ &= \frac{1}{2}\left\{\hat{1} + \lambda_1\begin{bmatrix}0 & 1\\ 1 & 0\end{bmatrix} + \lambda_2\begin{bmatrix}0 & i\\ -i & 0\end{bmatrix} + \lambda_3\begin{bmatrix}1 & 0\\ 0 & -1\end{bmatrix}\right\}.\end{aligned} \quad (25)$$

This decomposition allows us to express the three real degrees of freedom of the reduced density matrix as a real coherence vector $\vec{\lambda}_{\mathcal{S}} = [\lambda_1, \lambda_2, \lambda_3]$.

If the system is entangled with the environment, $\hat{\rho}_S^r$ represents a mixed state. Though, the entire system + environment remains in a pure state, information about any entanglement with the environment has been lost in the trace operation of Eq. (23). The coherence vector, like the reduced density matrix, contains only the information about the system cell that is local to that cell.

G. Polarization and coherence

The polarization operator for a two-dot QCA cell is the difference of the projection operators on the two dot-occupancy basis states, as visualized in Figure 2. Dots are numbered for reference. The polarization of the system cell is between −1 and 1, representing localization on one or the other dot.

$$\hat{P}_S = |1^S\rangle\langle 1^S| - |0^S\rangle\langle 0^S|, \tag{26}$$

$$P_S = \langle \hat{P}_S \rangle = \mathrm{Tr}\, \hat{\rho}_S^r \hat{\lambda}_3. \tag{27}$$

The expectation value of the electric dipole moment d of a cell about its center is proportional to the polarization, $d = eaP$.

The cell polarization is important in the QCA paradigm. In QCA circuit operation, the polarization encodes bit information. In conventional electronics a continuous real variable, the voltage on a conductor, is used to represent a binary value by segmenting its range into values that represent a logic level 1, a logic level 0, or a null (undetermined) value. So too in QCA, the continuous polarization of the cell encodes a binary value—a sufficiently positive polarization represents a binary 1, a sufficiently negative polarization represents a binary 0, and a polarization with a magnitude less than some threshold holds no information.

For the calculations reported here, we model the environment as cells with no tunneling between dots so the polarization of environment cells is always zero. The expectation value of the dipole moment of the environment cells is zero, as is the expectation value of the charge on each dot. Environment cells are in that sense neutral and unpolarized. In a mean field sense, they are electrostatically invisible. The environmental cells do not bias the system cell into one state or another. They can, however, still interact with the system cell Coulombically and become entangled with the system and with each other.

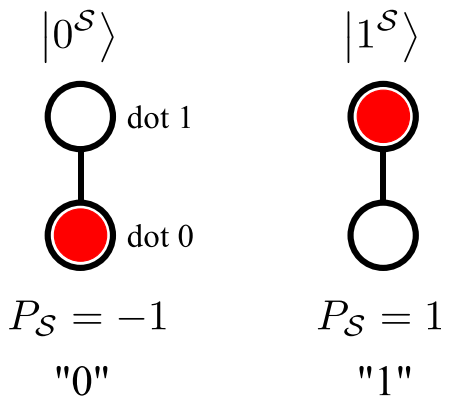

FIG. 2. Computational basis for the two-dot QCA system cell. Two completely localized, degenerate states of an isolated two-dot QCA cell provide a computational basis. Black circles represent the quantum dots, the intramolecular interdot tunneling path is indicated by a line connecting the two dots, and a red disc represents a mobile electron. A fixed, neutralizing charge of $+e/2$ is present at each dot but is not depicted. An electron localized on the top dot yields a cell polarization of $P = +1$ and represents a bit value of 1. An electron localized on the bottom dot yields a cell polarization of $P = -1$ and represents a bit value of 0.

H. Measures of coherence

We use several measures of the coherence or decoherence of a cell to capture the extent to which the cell's quantum state information has delocalized and has become entangled with the environment. The measures, we employ are the von Neumann entropy, the quantum mutual information between the cell and the environment, and the state purity.

The loss of local information results in an incomplete description of the central cell that is quantified through probabilities and the associated entropy. The reduced density matrix is Hermitian and so can be diagonalized by a unitary transformation. In this eigen-representation, the off-diagonal matrix elements are zero and the diagonal matrix elements are p_i, $i = 1, 2, \ldots, d$, where d is the dimension of the open system of interest. If all the p_i are zero except one, which must then be equal to 1, then the state is said to be a pure state. If not, it is a mixed state. The values of p_i can be interpreted as the probabilities of finding the system in the ith state. These probabilities are an expression of missing information.[17] For $\hat{\rho}_S^r$, the reduced density matrix of the system, the information is missing because some information is no longer local, but rather bound up in the entanglement with the environmental cells. For the complete density matrix of the system + environment, $\hat{\rho}$, by contrast, there is no missing information and it is always in a pure state as it evolves under Eq. (20).

The Shannon entropy S is a measure, defined on any set of probabilities p_i, that expresses how much information, measured in bits, is missing.[18] The missing information is what leads to a probabilistic description in the first place. Probabilities quantify partial information. If there were no missing information, there would be no need for probabilities.[12]

The Shannon entropy of the eigenvalues of a reduced density matrix $\hat{\rho}^r$ is known as the von Neumann entropy of the state (here measured in bits, instead of thermodynamic units). For the system cell this can be written

$$S_S = -\sum_{i=1}^{d} p_i \log_2(p_i) = -\mathrm{Tr}(\hat{\rho}_S^r \log_2 \hat{\rho}_S^r). \tag{28}$$

We denote the corresponding entropy of the environment $S_\mathcal{E}$ and of the whole system + environment as simply S. The von Neumann entropy measures the amount of information about the quantum state of the system cell that, while present in $\hat{\rho}(t)$, is missing from $\hat{\rho}_S^r(t)$. This loss of *local* quantum information is at the heart of decoherence.

Another measure of coherence, the quantum mutual information I, measures information (not missing information,

as in the case of entropy) that is present in the entanglement between two sub-systems. Applied to the cell and environment subsystems, we have

$$I_{\mathcal{SE}} = S_{\mathcal{S}} + S_{\mathcal{E}} - S. \tag{29}$$

The quantum mutual information $I_{\mathcal{SE}}$ is the difference between the quantum information that is missing from the individual subsystems, and that which is missing from the composite whole.

Because the QCA concept avoids using quantum information—it stores bits rather than qubits—the loss of local quantum information from the cell does not correspond to loss of information about the QCA bit.

State purity has often been used to quantify coherence. The purity of the cell is the expectation value of the reduced density operator itself. The purity $\nu_{\mathcal{S}}$ is defined as

$$\nu_{\mathcal{S}} = \mathrm{Tr}[\hat{\rho}^r_{\mathcal{S}}]^2. \tag{30}$$

This measure has the advantage of being straightforward to calculate even in large systems. A pure state has $\nu = 1$. If the number of degrees of freedom is d ($d=2$ for the 2-dot cell), a completely decoherent state has $\nu = 1/d$.

III. ISOLATED PURE STATE: EVOLUTION DOMINATED BY SYSTEM DYNAMICS

We consider first the limit in which the environment plays no role. A system in isolation, with no interaction with the environment ($N=0$ or $R=\infty$), is described by the system Hamiltonian $\hat{H}_{\mathcal{S}}$ alone; the environment Hamiltonian $\hat{H}_{\mathcal{E}}$ and the interaction $\hat{H}_{\mathcal{SE}}$ are both zero. The Hamiltonian governing this evolution is simply that of the system and has only the tunneling term connecting the two states.

$$\hat{H}_{\mathcal{S}} = \hat{H}^0_{\mathcal{S}} = -\gamma_{\mathcal{S}}\hat{\lambda}_1. \tag{31}$$

The time evolution of the system is dominated by Rabi oscillations for any initial state that is not a stationary state. The Rabi oscillation of this system is evident in Figure 3, which shows the time-varying polarization of the cell, the degree of freedom on which a bit is encoded. The Rabi oscillation occurs with period τ given by

$$\tau = \frac{\pi\hbar}{\gamma_{\mathcal{S}}}. \tag{32}$$

This period τ provides a characteristic time scale for the evolution of the system.

The time evolution of the system can be visualized by considering the motion of the coherence vector $\vec{\lambda}(t)$ as shown in Figure 4. The coherence vector for the fully coherent isolated system has unit length and so is always on the surface of the unit sphere, known as the Bloch sphere. The coherence vector's initial condition is marked in the figure by an arrow, and the path traced out by the tip in time is indicated by a curve. In this case, since the $\hat{\lambda}_1$ operator commutes with the Hamiltonian, the motion keeps λ_1 constant. Unitary evolution results in $\vec{\lambda}$ rotating around the λ_1-axis with a constant projection, for any initial state. The cell polarization is equal to the projection of $\vec{\lambda}$ on the $\hat{\lambda}_3$-axis. The stationary states are represented by $\vec{\lambda} = [\pm 1, 0, 0]$.

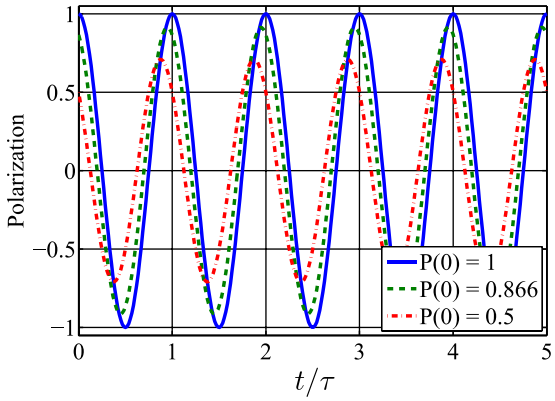

FIG. 3. Polarization oscillations and bit instability in an isolated system cell. The polarization of the system cell in isolation with tunneling energy $\gamma_{\mathcal{S}}$ exhibits Rabi oscillation with period $\tau = \pi\hbar/\gamma_{\mathcal{S}}$. Polarization is plotted in time for three different initial conditions: $\lambda_3^{\mathcal{S}}(0) = 1$ (solid blue trace); $\lambda_3^{\mathcal{S}}(0) = 0.866$ (dashed green trace); and $\lambda_3^{\mathcal{S}}(0) = 0.5$ (dashed and dotted red trace). Because QCA bit information is encoded in the sign of the polarization, perfectly coherent evolution results in periodic bit flips.

IV. DECOHERENCE: EVOLUTION DOMINATED BY ENVIRONMENTAL INTERACTIONS

A. Dynamics

We now consider the limit in which the system-environment interaction completely dominates system dynamics. Here, we take $\hat{H}_{\mathcal{S}} = 0$, so the Hamiltonian governing the evolution of the system-environment composite has two components

$$\hat{H} = \hat{H}_{\mathcal{E}} + \hat{H}_{\mathcal{SE}}, \tag{33}$$

where $\hat{H}_{\mathcal{E}}$ includes interactions among the environmental cells and $\hat{H}_{\mathcal{SE}}$ includes interactions between the system and the environment.

We calculate the unitary evolution of the whole system + environment in time using Eq. (20), and at each time

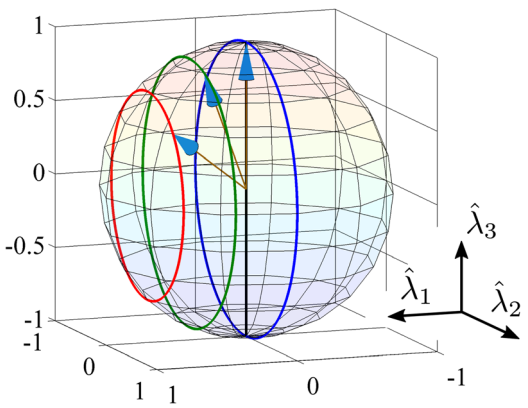

FIG. 4. The coherence vector $\vec{\lambda}$ of an of an isolated system cell. The evolution in time is shown for the same conditions as in Figure 3. In each case, the coherence vector traces out a circle in on the unit sphere with constant λ_1.

explicitly calculate the reduced density matrix for the system using Eq. (23), and for the environment using Eq. (24). The coherence vector, cell polarization, and other measures can be calculated from either the full density matrix or the reduced density matrices.

For the response of the system to the environment, we choose a time scale based on the strongest possible interaction E_e^{flip} between the system cell and a cell on the environmental sphere of radius R. E_e^{flip} is determined by the bit flip energy as defined in Eq. (17) and reduces to the expression

$$E_{\text{e}}^{\text{flip}} = \frac{e^2}{4\pi\epsilon_o}\left(\frac{1}{R} - \frac{1}{\sqrt{R^2 + a^2}}\right). \tag{34}$$

In an environment of many cells, there is likely a cell that interacts with the system with an energy approaching E_e^{flip}. The corresponding characteristic time for environmentally–induced changes is

$$\tau_e = \frac{2\pi\hbar}{E_e^{\text{flip}}}. \tag{35}$$

Figure 5 illustrates that the polarization in this case is constant in time for any initial value, in contrast to the Rabi oscillations seen in Figure 3. Since the system cannot switch, this is hardly surprising. Far more interesting behavior is revealed when we examine the full coherence vector and various coherence measures.

Figure 6 shows the temporal evolution of the coherence vector for several initial states. In each case, interaction with the environment causes the coherence vector to move toward the $\hat{\lambda}_3$ axis. The λ_1 and λ_2 components do not vanish linearly, but they die out quickly, being almost entirely gone by $t = \tau_e/10$. Figure 7 shows the λ_1 and λ_2 components of the system cell as a function of time for the case when the initial polarization is zero ($\lambda_3(0) = 0$) and Figure 8 shows these coherence vector components for the environmental cells. Note that the environment cells have $\lambda_3 = 0$ always.

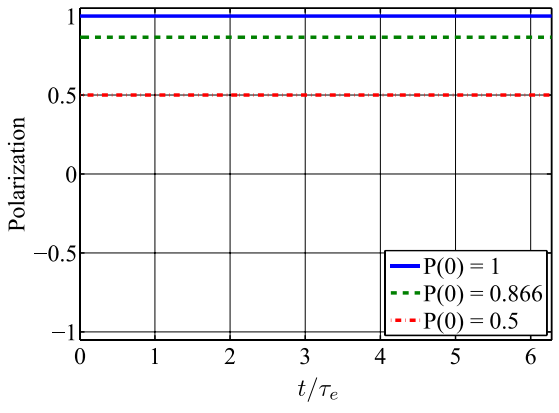

FIG. 5. Bit stabilization in a system dominated by the environmental interaction. The system cell polarization is shown as a function of time for the same three initial conditions as those for the isolated system shown in Figures 3 and 4. In this case, however, there are $N = 8$ randomly positioned and oriented environmental cells distributed on a sphere of radius $R = 3.375\,a$ (a is the interdot distance). Plotting just the polarization masks much of the underlying behavior, however. Figure 6 represents the same temporal evolution as in this calculation, but displays the coherence vector of the system.

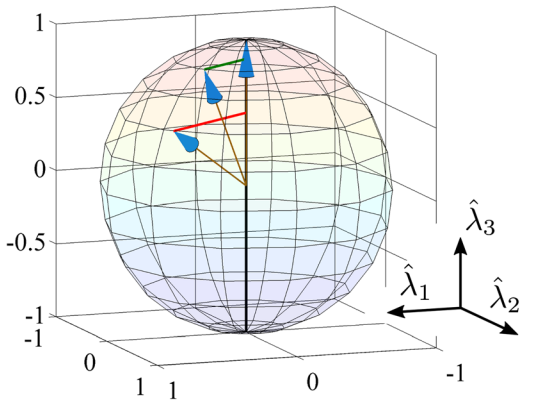

FIG. 6. Time evolution of the system coherence vector $\vec{\lambda}$ when the environmental interaction dominates. This is the same calculation, with the same three initial states ($P = 1$, 0.866, and 0.5) as is shown in Figure 5. The environment consists of $N = 8$ cells on a sphere of radius $R = 3.365\,a$. The system cell's time evolution is indicated by the curve traced out by the tip of the coherence vector in time. Here, the cell maintains constant polarization (the bit is stabilized with constant λ_3), but quantum coherence is destroyed as coherence vector components λ_1 and λ_2 decay to zero. This corresponds to the decay of the off-diagonal elements of the reduced density matrix $\hat{\rho}'_S$. The system + environment remains in a pure state undergoing unitary evolution. The $\hat{\lambda}_3$ axis is the locus of Zurek pointer states. Decoherence drives the system into the classical subspace of these pointer states.

The behavior illustrated here can be understood in terms of the decoherence paradigm of Zurek.[11] The system cell is being driven to the $\hat{\lambda}_3$ axis by its interaction with the environment. States on the $\hat{\lambda}_3$ axis are "pointer states," in Zurek's terminology. (The term originates in idea is that pointer states are those which are represented by the needle pointer on a laboratory gauge.) Both system and environmental states lose coherence, move off the surface of the Bloch sphere, and are driven to the subspace of pointer states. The selection of a particular set of these preferred system states is called einselection (*e*nvironmentally *in*duced *selection*).

What determines, which states are pointer states? Why is this one axis of the Bloch sphere singled out? The cell polarization is an observable corresponding to the operator

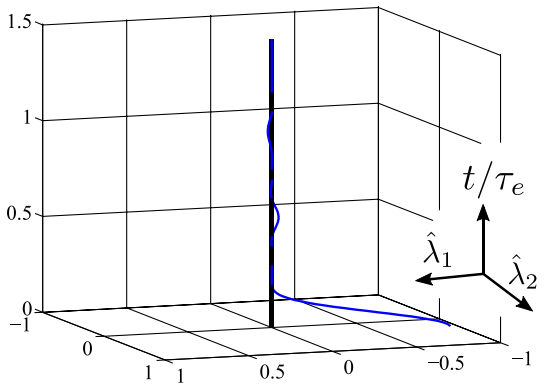

FIG. 7. Decoherence of the system due to interaction with the environment. The double-dot system cell here initially is in an unpolarized ($\lambda_3 = 0$) but fully coherent state. Interaction with the environment causes the λ_1 and λ_2 components to decay, though not monotonically. The environment here is the same as for the simulations shown in Figures 5 and 6 ($N = 8$ and $R = 3.365\,a$).

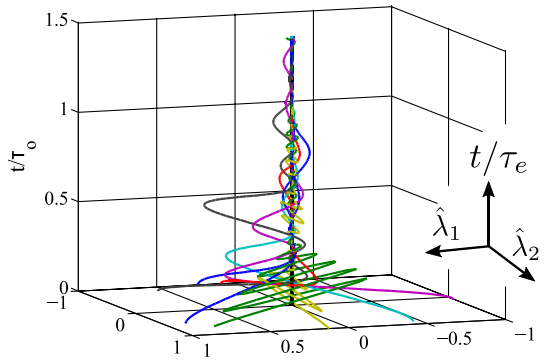

FIG. 8. Decoherence of the environment cells. Just as the system cell undergoes decoherence, so do the environment cells. For the same time evolution shown in Figure 7, the λ_2 and λ_3 components of the $N=8$ environment cells are shown as functions of time. The somewhat slower decoherence of the environment cells, compared to the system cell, is due to the fact that in this model geometry, environmental cells have fewer close neighbors than the system cell (see Figure 1). The system + environment remains in a pure state throughout.

$$\hat{P} = \hat{I}_{\mathcal{E}} \otimes \{\hat{\lambda}_3\}_{\mathcal{S}}, \tag{36}$$

in the full system + environment Hilbert space. This observable commutes with the interaction Hamiltonian.

$$[\hat{P}, \hat{H}_{\mathcal{SE}}] = 0. \tag{37}$$

The interaction Hamiltonian will therefore leave states in this subspace unaltered. This is a fundamental insight of Zurek's decoherence theory—the eigenspace of operators which commute with the interaction Hamiltonian are einselected for local survival by the environment. Other states decohere rapidly, which means they become entangled with the environment and cannot be represented by local quantum information.

This is decoherence, not measurement. Figure 6 might suggest "projection," but in reality there is no projective measurement happening here, just unitary evolution of the whole system + environment. The overall state remains a single coherent state. Decoherence explains why the pointer state subspace is selected, but not why a specific value (of position, say) would be the result of a particular measurement event. The probabilities remain, describing potential outcomes of measurements. Decoherence does not solve the "measurement problem" of quantum mechanics—why a particular outcome occurs in a specific measurement and other possible outcomes do not.

B. Entropy and information

We directly calculate the von Neumann entropy of the system from the reduced density matrix using Eq. (28). We also calculate the reduced density matrix of the environment at each point in time, and find the corresponding entropy. The von Neumann entropy, calculated from the complete density matrix $\hat{\rho}(t)$, of the entire system + environment is always zero.

If the system is initially fully polarized ($P = \lambda_3 = 1$), then the interaction with the environment has no effect: the coherence vector remains on the $\hat{\lambda}_3$ axis and there is no change in the entropy.

The other limit is more interesting. Suppose, the system is initially on the $\vec{\lambda}_3 = 0$ circle (the equator of the Bloch sphere). In this case, there is no QCA bit information in the system; it is in the QCA "null" state. The system nevertheless holds local quantum information in its quantum state. This information entangles with the environment and is lost to the system under unitary evolution of the system + environment.

Figure 9 shows three quantum information measures evolving in time due to the interaction of the system with the environment: the system entropy $S_{\mathcal{S}}(t)$, the environment entropy $S_{\mathcal{E}}(t)$, and the quantum mutual information $I_{\mathcal{SE}}(t)$. The system is initially in the $\vec{\lambda} = \hat{\lambda}_1$ state. Both system and environment start in coherent states with zero entropy, i.e., no information is missing from the local description provided by the reduced density matrix. The quantum mutual information is initially zero because the system and environment are unentangled. As the system interacts with the environment and becomes entangled with it, one bit of local information goes missing from the system and so the system entropy rises to one bit. Similarly, local information is lost from the environment and the environmental entropy climbs accordingly (in a bipartite system, these must mirror each other[19]). These two bits missing locally from the system and environment are manifest in the entanglement of the system with the environment in the form of the quantum mutual information, which rises to two bits. There is no information missing from the system + environment taken as a whole, so its entropy remains zero throughout.

We emphasize that QCA bit information is different from quantum information and is unaffected by decoherence in this case. The cell polarization is preserved as decoherence drives the system into the pointer states. This is because the pointer states are precisely those which encode QCA information.

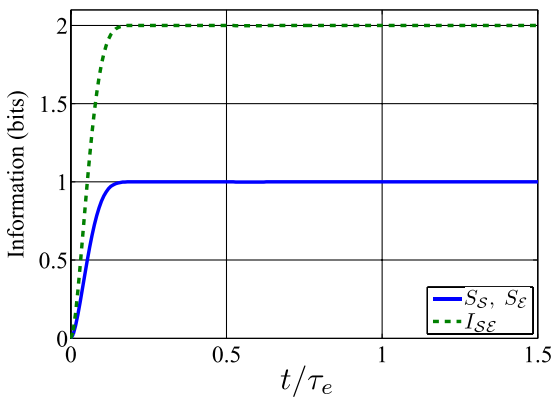

FIG. 9. The loss of local information from the system cell and the environment. The entropy and quantum mutual information are shown for the same temporal evolution as described in Figures 7 and 8. The system cell is initially unpolarized with $\vec{\lambda}(t=0) = \hat{\lambda}_1$. The system + environment evolves under the Hamiltonian of Eq. (33), causing decoherence in both the system and the environment. The von Neumann entropy of the system $S_{\mathcal{S}}$ and the entropy of the environment $S_{\mathcal{E}}$ both increase as entanglement and decoherence proceed. One bit of local quantum information goes missing from the system $\mathcal{S}$ and one bit goes missing from the environment $\mathcal{E}$. Correspondingly, two bits are manifested in the entanglement between $\mathcal{S}$ and $\mathcal{E}$ in the form of quantum mutual information $I_{\mathcal{SE}}$.

V. THE GENERAL CASE: SYSTEM DYNAMICS COMPETE WITH ENVIRONMENTAL INTERACTIONS

We consider the more general case where both internal dynamics and coupling to the environment play a role. The Hamiltonian, given by Eq. (10), includes tunneling between the system cell dots, Coulomb interaction with environmental cells, and the Coulomb coupling between environmental cells. As in the previous two cases, the environmental cells have no net charge or electric dipole moment, and have no internal dynamics.

A. Dynamics

The relative strength of the internal dynamics and the environmental coupling can be quantified by the ratio of the characteristic times, or equivalently, the ratio of energies. We define this ratio as follows:

$$\chi \equiv \frac{\tau}{\tau_e} = \frac{E_e^{\text{flip}}}{2\gamma_S}. \tag{38}$$

The isolated system considered in Sec. III corresponds to $\chi = 0$, while the system which is completely dominated by environmental interactions, as in Sec. IV, has $\chi = \infty$. In this section, we consider finite values of $\chi > 0$.

The effect of entanglement with even a one-cell environment is striking. Figure 10 shows the polarization as a function of time for a system cell in the presence of one environmental cell at $R/a = 1.5$. The entanglement suppresses the Rabi oscillations, so that the polarization does not change sign, which is important for QCA operation.

A larger environment ($N = 8$) stabilizes the oscillations more, as shown in Figure 11 for several initial polarizations. The corresponding evolution of the coherence vector is shown in Figure 12. These are to be compared with Figures 3 and 4, for the case of an isolated cell, and Figures 5 and 6, for the case of a cell with only environmental decoherence and no internal dynamics. In the present intermediate case, the system cell substantially decoheres, but not completely, with some small coherent oscillations continuing indefinitely. The coherence vector in this case moves rapidly off the Bloch sphere, in a time characterized by τ_e, and approaches the $\hat{\lambda}_3$ axis, but does not go all the way to the axis.

The strength of the interaction between the system cell and the environment varies as the radius R changes. Figure 13 shows the system polarization for various values of R. The ratio χ varies from $\chi = 0.12$ for $R/a = 7.6$, the weakest interaction shown, to $\chi = 11.5$ for $R/a = 1.5$, the strongest interaction. It is clear that the stronger the interaction, the more the polarization is stabilized and Rabi oscillations are suppressed.

Figure 14 shows the magnitude of the effect of variations in the specific orientational configuration of the environment,

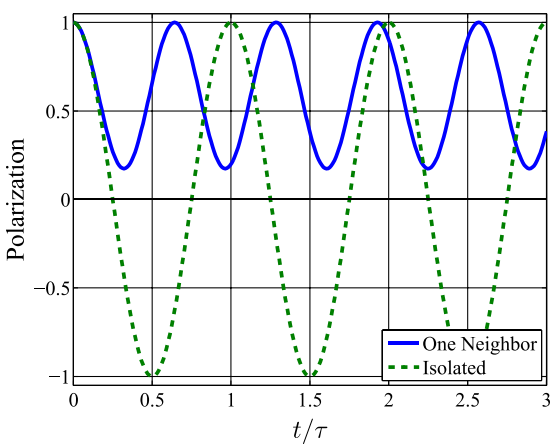

FIG. 10. Bit stabilization for a system cell in a minimal environment. In the presence of a single environment cell, Rabi oscillations in the system cell are sufficiently reduced that the polarization maintains its sign, and thus the QCA bit is stabilized. In this case, the environment cell is aligned with the system cell at $R = 1.5\,a$, for which $\chi = 1.54$. The polarization of the system cell in isolation, with only internal system dynamics, is also shown (green dashed trace) for comparison.

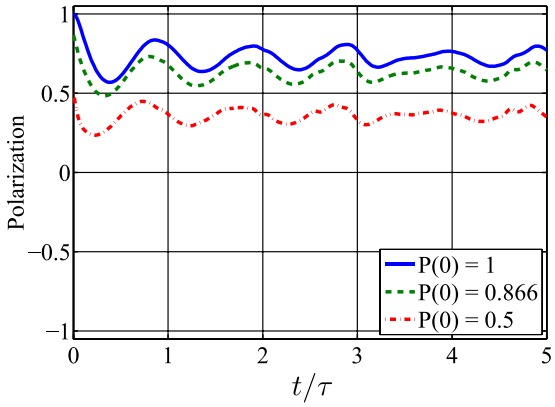

FIG. 11. Competition between Rabi oscillations due to internal dynamics and environmental decoherence. An $N = 8$ cell environment with $R = 3.38\,a$ causes the system cell to partially decohere, but with residual oscillations. This plot of the system cell polarization for several different initial values, can be compared to Figure 3, which shows the case of no environment ($\chi = 0$), and Figure 5 for the case of a dominant environment ($\chi = \infty$). Here, the situation is intermediate with $\chi = 1.2$. The effect of environmental decoherence is to stabilize the QCA bit value represented by the sign of the polarization.

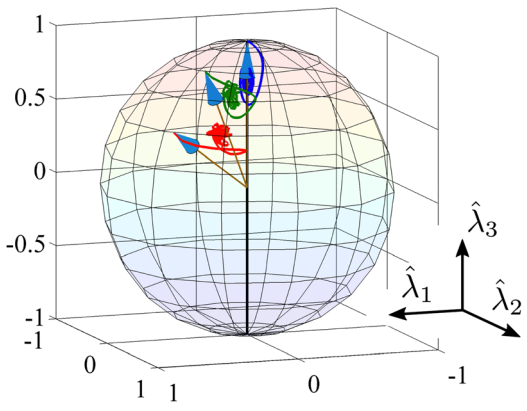

FIG. 12. The time evolution of the coherence vector for the case when environmental decoherence competes with system-driven oscillations. The coherence vector, shown here for three different initial states, quickly moves off the surface of the Bloch sphere and toward the $\hat{\lambda}_3$ axis. The long-term behavior retains some oscillatory character and, in contrast with the environmentally dominant case shown in Figure 6, the coherence vector is not driven completely to the pointer states on the axis. The environment consists of $N = 8$ cells randomly arranged and randomly oriented on a sphere of radius $R = 3.38\,a$, yielding a ratio $\chi = 1.2$.

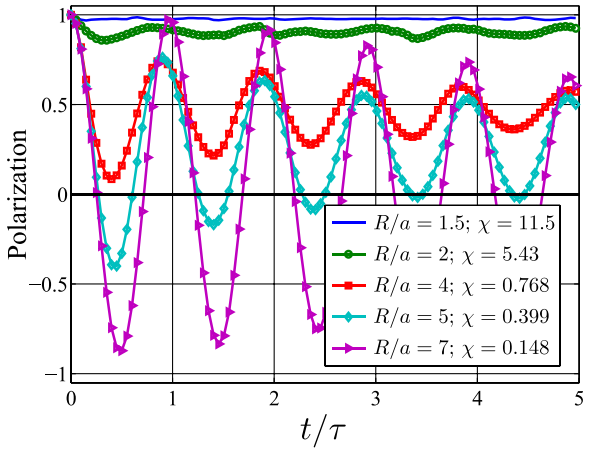

FIG. 13. Effect of varying the coupling to the environment. Bit stabilization weakens as the system-environment interaction is reduced by extending the radius R of the eight-cell ($N = 8$) sphere of environmental cells (see Figure 1). Rabi oscillations becomes the dominant feature of system cell dynamics. On the other hand, as R is reduced, bit stabilization improves, with a higher asymptotic value and reduced fluctuation. This is the limit where system-environment interactions dominate internal system dynamics and approaches the situation shown in Figure 5.

and Figure 15 shows the polarization for a larger environment, here with $N = 26$ cells. More cells also means, of course, a stronger total coupling between the system and the environment. Calculating the response with this many cells is only tractable using the analytic results of the Appendix.

B. Pointer states

For strong environmental decoherence (large χ), we have seen that the system is driven into the subspace of pointer states, which here are along the $\hat{\lambda}_3$ axis. We can see how as χ decreases, the system smoothly transitions from this behavior to regular oscillatory motion, when the internal system dynamics dominate, by examining the long-time limit of the coherence vector motion. An analytic expression, Eq. (A16), for the time dependence of the coherence vector in this general case is derived in the Appendix. At long

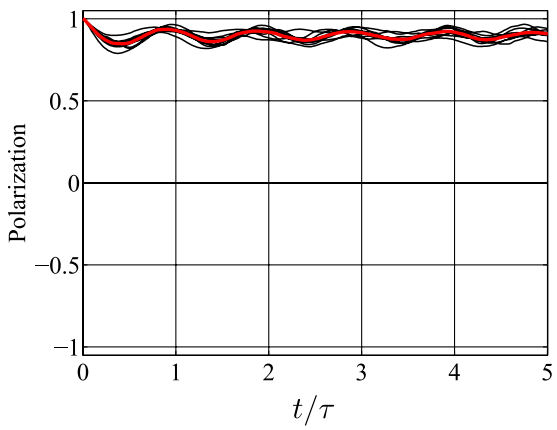

FIG. 14. Effect of the random configuration of the environment cells. The ten individual black traces each show the time-varying polarization of a system cell interacting with an eight-cell environment ($N = 8$) of radius $R = 2.95\,a$ ($\chi = 3.94$) for a random configuration of ten environment cells. The red trace is the average of these.

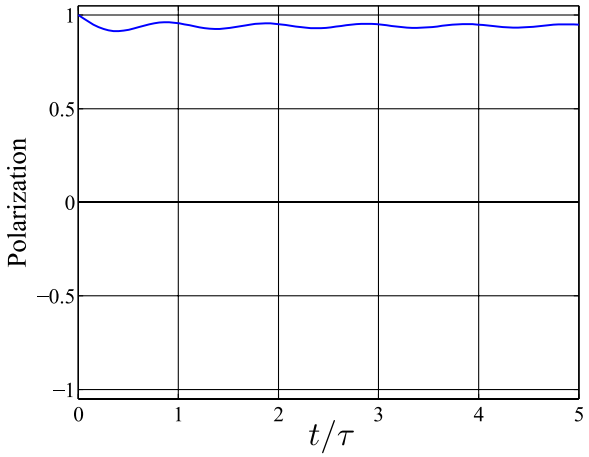

FIG. 15. Calculated polarization for a large environment. The time-varying polarization for a system interacting with an environment composed of $N = 26$ cells around a radius $R = 2.75\,a$ yielding $\chi = 4.5$. This result is calculated using the analytical results of Eq. (A16).

times, the motion oscillates around a point in the $\hat{\lambda}_1$—$\hat{\lambda}_3$ plane, which depends on the initial value of $\vec{\lambda}$.

The locus of these limit points changes when χ changes, as shown in Figure 16. Note that the lines in the figure show

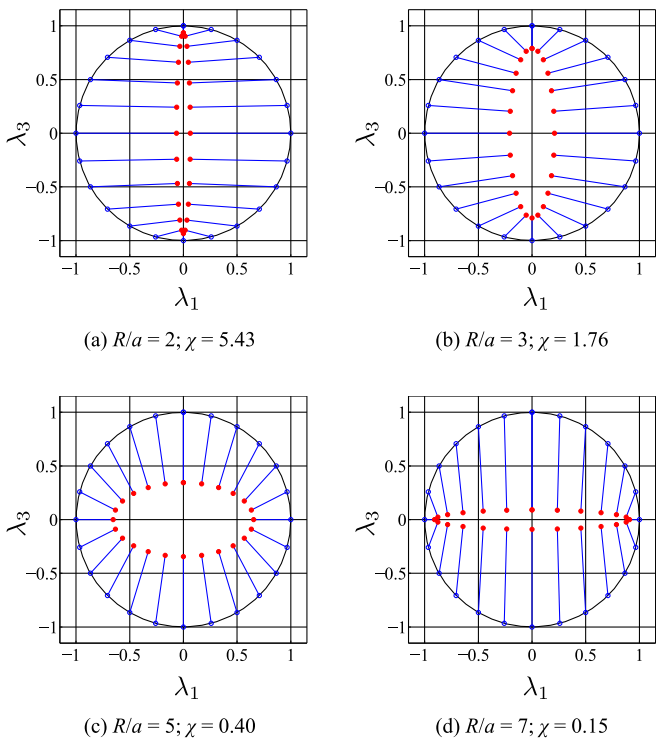

FIG. 16. Dependence of asymptotic value upon the relative influence of internal system dynamics and system-environmental interaction. Asymptotic values of λ_1 and λ_3 are plotted for various system cell initial conditions of the form $\vec{\lambda}(0) = (\lambda_{1,o}, 0, \lambda_{3,o})$. Initial states are marked by a blue open circle, and all start on the Bloch sphere (black circle). Asymptotic states are denoted by a red dot, with each linked by a blue line to its initial state. This illustrates only the connection between the initial state and the asymptotic state—not the full temporal evolution. In the limit of dominant system-environmental interaction ($\chi \to \infty$), asymptotic values lie on the λ_3 axis, with λ_3 as a constant of motion, yielding perfect environmental bit stabilization. In the limit of dominant system internal dynamics $\chi \to 0$, the λ_1 system degree of freedom is a constant of motion as the system undergoes Rabi oscillation about the λ_1 axis.

the association of each limit point with the initial $\vec{\lambda}$ value, but do not represent the actual evolution of $\vec{\lambda}$. For large χ, the limit points are very near the $\hat{\lambda}_3$ axis, and are approached rapidly as the system decoheres and oscillations become small. These states represent the classical pointer states. As the environmental coupling χ decreases, the limit points move away from the $\hat{\lambda}_3$ axis and oscillatory behavior emerges. For very small χ, the limit points are near the $\hat{\lambda}_1$ axis and the motion becomes dominated by Rabi oscillations in planes perpendicular to the $\hat{\lambda}_1$ axis, approaching the isolated system limit shown in Figure 3.

C. Entropy and information

We examine again the loss of local quantum information that accompanies decoherence. As in the case shown in Figure 9, we examine the situation when the cell polarization is initially zero and $\vec{\lambda}(t=0) = \hat{\lambda}_1$. Figure 17 shows the movement of information out of local degrees of freedom in the system and into the entanglement with the environment. The missing local information, quantified by the system entropy, increases as a result of environmental interaction on a time-scale determined by τ_e. As in the previous case, the information missing from the local system (the system entropy) is exactly equal to that missing from the environment (the environmental entropy). The net missing local information shows up in the quantum mutual information, which captures information which resides in neither system nor environment, but rather in the entanglement between the system and the environment. The effect of the competition between environmental decoherence and local system dynamics is seen in that the entropy does not increase to a full bit, and there are non-monotonic mini-revivals when the information of entanglement briefly returns to the system.

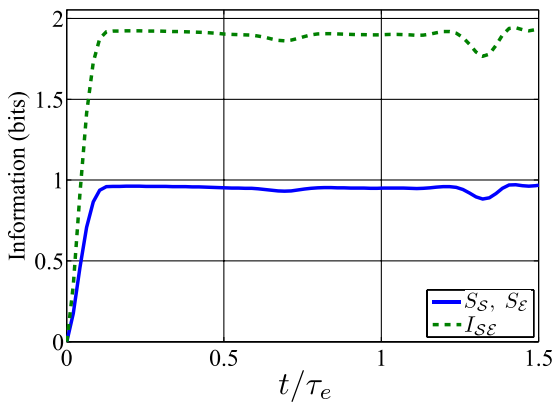

FIG. 17. Loss of local information from the system cell and the environment for the situation where local dynamics and decoherence are competing with each other. As was the case shown in Figure 9, the system interacts with the environment and they become entangled, with a resulting loss of local information. Here, the value of the ratio χ, which quantifies the relative strengths of the internal dynamics and system-environment interaction (Eq. (38)), has the value 1.26; for the situation shown in Figure 9, χ is infinite. There is an increase in the system entropy S_S and the environmental entropy $S_\mathcal{E}$, which each express the amount of missing local information. This information appears in the entanglement of the system with the environment, represented by the quantum mutual information $I_{S\mathcal{E}}$. The result of the non-zero local dynamics is that somewhat less than one full bit of local quantum information goes missing from both the system and the environment. In the limit, where $\chi = 0$, i.e., no coupling to the environment, no information would leave the system, resulting in a constant $S_S = S_\mathcal{E} = 0$. Here, brief mini-revivals are also evident, when information returns from the entanglement to the local systems. The entropy of the full system + environment is always zero.

VI. A LARGER SYSTEM: THE FOUR-DOT CELL

A. Geometry and polarization

In actual QCA circuits information is rarely held in a single cell, but rather in QCA bit packets comprised of several cells.[20] We here consider the simplest extension in that direction—a four-dot cell composed of two parallel double-dot cells with the four dots forming a square, as shown in Figure 18. The QCA information is now distributed over two cells.

The polarization of the four-dot cell is defined in terms of the projection operators onto each of the four dots.

$$\hat{P} = \frac{\hat{P}_2 + \hat{P}_3 - \hat{P}_1 - \hat{P}_4}{\hat{P}_1 + \hat{P}_2 + \hat{P}_3 + \hat{P}_4}. \tag{39}$$

Here

$$\begin{aligned} \hat{P}_1 &= |1^L\rangle\langle 1^L| \otimes \hat{1}^R, \\ \hat{P}_2 &= |0^L\rangle\langle 0^L| \otimes \hat{1}^R, \\ \hat{P}_3 &= \hat{1}^L \otimes |1^R\rangle\langle 1^R|, \quad \text{and} \\ \hat{P}_4 &= \hat{1}^L \otimes |0^R\rangle\langle 0^R|. \end{aligned} \tag{40}$$

The operator $\hat{P}$ acts in the four-dimensional Hilbert space of the density matrix $\hat{\rho}_S$ (or reduced density matrix $\hat{\rho}_S^r$) of the four-dot cell. The cell polarization is proportional to the electric quadrupole moment around the cell center. The Coulomb interaction favors alignment of neighboring four-dot cells with the same polarization.

B. Internal system dynamics

For an identical coupling between dots, the four-dot cell in isolation exhibits Rabi oscillations with a longer period than the two-dot cell. Figure 19 compares the polarization oscillations for an initially fully polarized four-dot and two-dot cell.

The longer Rabi oscillation period is due to a higher effective kinetic barrier between the two polarization states. To switch from a $P = 1$ state to the energetically degenerate $P = -1$ state, the four-dot cell must go through a higher-

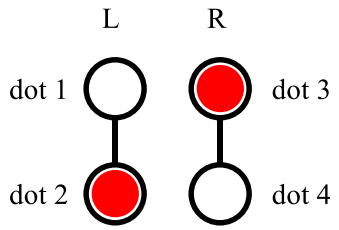

FIG. 18. Four-dot QCA cell. A four-dot QCA cell is comprised of two parallel two-dot cells. The four dots form a square, and they are numbered 1–4 for reference, with individual two-dot cells labeled "L" and "R".

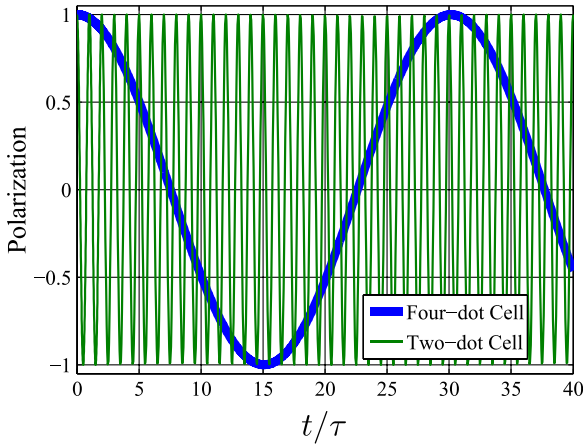

FIG. 19. Slower internal system dynamics of a four-dot cell. Rabi oscillations in the cell polarization of a two-dot cell is compared with those of a four-dot cell comprised of identical two-dot cells. Both systems have the same interdot tunneling energy. The Rabi oscillation period τ of the two-dot cell provides the time scale. The slower intrinsic response of the larger system is due to the additional kinetic barrier for switching.

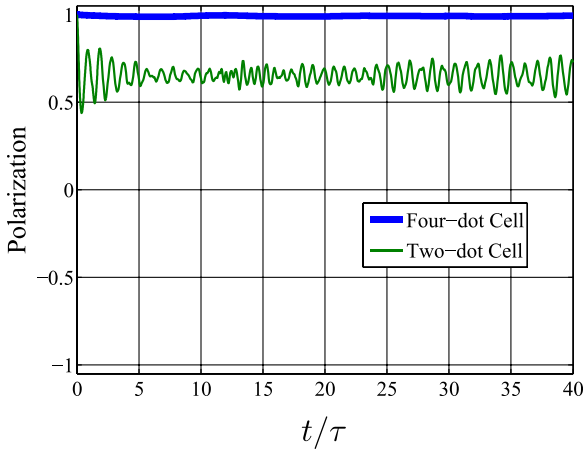

FIG. 20. Enhanced bit stabilization in a four-dot cell. The polarization as a function of time is shown for both a two-dot cell and four dot cell with the same inter-dot tunneling dynamics. Each is allowed to interact with an identical seven-cell environment with $\chi = 1.26$. Decoherence with the environment is more effective at stabilizing the larger system against coherent Rabi oscillations.

energy "kink" state in which both mobile electrons are on the top (or bottom) of the cell.

This enhanced kinetic barrier for switching is a general feature of longer multicell bit packets as well. For example, for a packet composed of four four-dot cells to switch from $[+1, +1, +1, +1]$ to $[-1, -1, -1, -1]$ (labeling cell by its polarization) it must go through intermediate states such as

$$[+1,+1,+1,+1] \rightarrow [-1,+1,+1,+1] \rightarrow [-1,-1,+1,+1] \rightarrow [-1,-1,-1,+1] \rightarrow [-1,-1,-1,-1].$$

The three intermediate states have higher energy than the initial or final states. The longer the bit packet, the "wider" is the effective kinetic barrier to switching, and the longer is the corresponding Rabi oscillation time. This longer characteristic oscillation time has as a consequence that environmental decoherence will have more time in which to drive the system into the subspace of pointer states.

C. System internal dynamics in competition with the system-environment interaction

We compare the effect of the environment, as modeled in Sec. II, on the four-dot and two-dot QCA cells. Figure 20 shows the effect of an identical environmental configuration, with $N = 7$, $R/a = 3.375$, $\chi = 1.26$, on initially–fully polarized four-dot and two-dot cells. The cell interdot tunneling energies, defined by Eq. (2), are identical for both cells. The Rabi oscillations for the four-dot cell are clearly more suppressed by interaction with the environment than for the two-dot cell.

The enhanced environmental bit stabilization for the larger system can be understood as a consequence of the inherent bistability of the two (or more) electron system. This bistability plays the role in QCA circuits that voltage gain plays in conventional devices. (Power gain is a feature of clocked QCA system, see Ref. 21).

The decoherence paradigm provides another view on the enhanced stability: the fragility of quantum information in extended systems. The larger four-dot system has more ways to interact with the environment and entanglement is more effective at removing local quantum information than for the smaller system. Figure 21 shows the system entropy (missing information) in the two and four-dot systems with identical environments, shown here, as with Figure 17, for initially unpolarized cells. Of course, the larger system has more quantum information: two bits rather than one. More important to note is that (a) the quantum information is lost from the system faster in the four-dot cell and (b) it stays lost more completely, showing smaller signs of quantum revivals.

Figure 22 shows a comparison of another measure of decoherence, the system purity. The four-dot cell has a minimum purity of 1/4 and the two-dot cell has a minimum purity of 1/2. Decoherence drives the larger system to its minimal purity and keeps it very close to that.

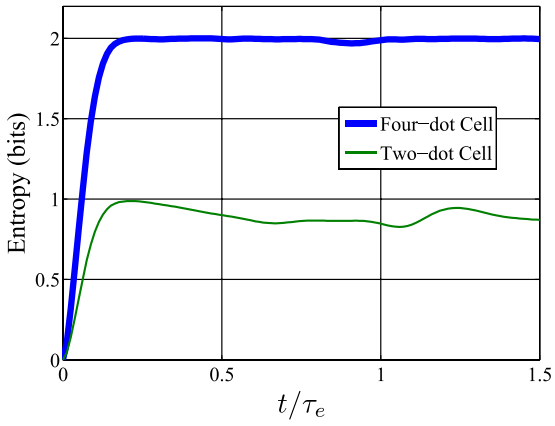

FIG. 21. System entropy of a decohering four-dot cell compared with a two-dot cell. The four-dot cell and the two-dot cell interact with identical environments and have the same interdot tunneling energy γ. The von Neumann entropy of the four-dot cell rises faster and saturates more closely to its maximum entropy value (two bits) than does the two-dot cell, which has a maximum entropy of one bit.

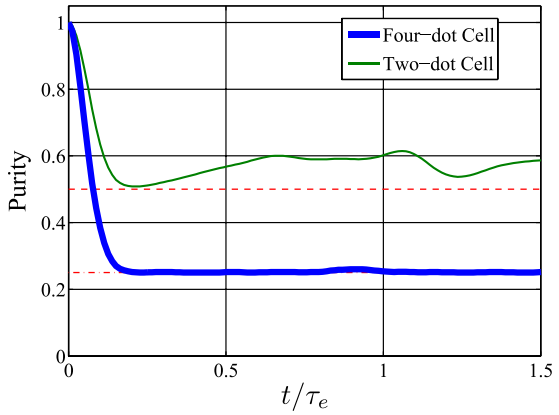

FIG. 22. Quantum purity of a decohering four-dot cell compared with a two-dot cell. The four-dot cell and the two-dot cell interact with identical environments and have identical interdot tunneling energies. The larger four-dot cell's quantum purity falls faster and settles more closely to its minimum purity value ($\nu_{\min} = 0.25$, dashed and dotted red line) than does the two-dot cell's purity ($\nu_{\min} = 0.5$, dashed red line), indicating a more rapid and more complete decoherence for the four-dot cell than for the two-dot cell.

VII. DISCUSSION

Quantum information is inherently fragile. By quantum information, we here mean of course, quantum information local to the system. In most quantum computing approaches, maintaining quantum coherence throughout the system is desirable. The fragility of quantum information is due to the fact that any interaction with the environment can result in a loss of system coherence.

Loss of coherence in the system *is* the entanglement of the system with environmental degrees of freedom. As a result of this entanglement, though the system + environment together maintain a unitary time evolution, the best local description of the system itself, the reduced density matrix, looses quantum information. This information loss is quantified by in an increase in the Von Neumann entropy of the system measured in bits; the entropy is the amount of information that is missing locally. In our model, we see that missing information showing up in the quantum mutual information between the system and environment.

The QCA approach is less ambitious than quantum computing and seeks to encode only classical bit information in the system. Quantum mechanical tunneling is crucial for the time evolution of QCA circuits, but the bit information itself is encoded in the sign of the cell polarization, a classical degree of freedom. In this context Rabi oscillations, which can flip the sign of the polarization, are a good thing for quantum computing—they show that system coherence is being preserved—but are problematic for QCA because they can cause a loss of QCA information. Von Neumann entropy measures the degree to which quantum, not QCA information, has gone missing.

Decoherence, which is deadly for quantum computing, is revealed to be a friend to QCA. We have seen (Figure 10) that even a single environmental cell can suppress Rabi oscillations and stabilize QCA bit information. Larger environments provide even more stabilization (Figure 15). The interaction with the environment tends to drive the system into the Zurek pointer states. For QCA, the pointer states are precisely the information-encoding states of definite polarization. The fundamental reason for this is that QCA encodes information in the spatial position of particles. The Coulombic interaction Hamiltonian with charges in the environment is a function of the position operator, so position eigenstates are einselected by this interaction and become the pointer state subspace. (Other environmental interactions are possible, of course, but here the Coulomb interaction dominates.)

To assess the exact balance between internal dynamics—which produces oscillations—and decoherence requires a knowledge of χ from the specifics of the environment. It is nevertheless clear that coherence is very difficult to maintain (a fact well known in quantum computing) and that the effect of decoherence is to stabilize QCA-encoded bits. As the system becomes larger, as in a multi-cell bit packet, the stability increases, as shown in Figure 20.

We have explored the limits of complete isolation ($\chi = 0$), domination by environmental decoherence ($\chi = \infty$), and competition between the internal system dynamics with intermediate values of χ. An environment at non-zero temperature would cause even more rapid decoherence. We have not here examined the situation where the environment can exchange not only information, but also energy, with the system. This has been done using small cellular models,[21] phenomenological models,[22] and correlation expansions of Mahler.[16,23] The present discussion has also not included clocked QCA cells and memories. These remain for future work.

ACKNOWLEDGMENTS

This material was based on work supported by the National Science Foundation under CHE-1124762, and was conducted with support under and awarded by DoD, Air Force Office of Scientific Research, National Defense Science and Engineering Graduate (NDSEG) Fellowship, 32 CFR 168a.

APPENDIX: THE DEVELOPMENT OF ALGEBRAIC EXPRESSIONS FOR THE EVOLUTION OF THE SYSTEM CELL'S COHERENCE VECTOR

An analytic form for the evolution of the system cell's coherence vector will allow us to calculate the dynamics of a system cell in interaction with an environment larger than practicable for simulation on currently available resources, and it allows the determination of the center of motion of the system cell's coherence vector. To this end, we outline the algebra behind the development of expressions for the dynamics of the system cell's coherence vector. We perform this analysis in two regimes: first, in the limit of dominant system-environment interaction over system internal dynamics ($\gamma_S = 0$), resulting in perfect bit stabilization; and, second, in the regime where system internal dynamics competes with system-environment interaction to determine the time variance of the system cell's coherence vector. In each case, we assume a unicellular system cell with a two-cell environment, since this three-cell system-environment composite provides the generality of an N-cell environment (here, $N = 2$) with minimal algebraic complexity. The environmental cells

will be fixed in a depolarized state to provide a minimal, charge-neutral environment having several quantum degrees of freedom with which the system may entangle.

For both regimes as discussed above, the same basis is used, and the first two steps are identical. We first describe the basis for the calculation. Then, we list the equation of motion, establish the initial condition, and finally show the analytic form for the system cell's coherence vector obtained from both Mathematica® and direct analysis.

1. Basis kets

We use as the basis kets $|\psi\rangle$ those kets formed by taking the direct product of the various combinations of computational basis kets $\{|0\rangle, |1\rangle\}$ for the individual cells. The basis kets for the individual cells are states in which the cell's single mobile electron is completely localized to dot m ($m \in \{0,1\}$): $B^{\mathcal{S}} = \{|0^{\mathcal{S}}\rangle, |1^{\mathcal{S}}\rangle\}$ in the Hilbert space of the system; and $B_1^{\mathcal{E}} = \{|0_1^{\mathcal{E}}\rangle, |1_1^{\mathcal{E}}\rangle\}$ and $B_2^{\mathcal{E}} = \{|0_2^{\mathcal{E}}\rangle, |1_2^{\mathcal{E}}\rangle\}$ in the respective Hilbert spaces of the two environment cells, numbered 1 and 2. Our ordered basis B for simulating the coherent evolution of the three-cell composite, then, is $B = \{|\psi_{m_0;\vec{m}_p}\rangle\}$, where m_0 identifies a computational basis state for the system, and $\vec{m}_p = [m_1, m_2]$, with $m_k \in \{0,1\}$, specifies an environmental basis state

$$\vec{m}_p = [m_1, m_2] \quad \leftrightarrow \quad |(m_2)_2^{\mathcal{E}}\rangle|(m_1)_1^{\mathcal{E}}\rangle. \tag{A1}$$

Here, we use the shorthand notation $|\alpha\rangle|\beta\rangle$ for the direct product $|\alpha\rangle \otimes |\beta\rangle$. The subscript $p \in \{1,2,\ldots,N_{\mathcal{E}}\}$ assigns a counting number to each of the $N_{\mathcal{E}} = 2^N$ environmental basis states. For our three-cell composite, the basis kets of B take the form

$$\begin{aligned}
|\psi_{0;[0,0]}\rangle &= |0_2^{\mathcal{E}}\rangle|0_1^{\mathcal{E}}\rangle|0^{\mathcal{S}}\rangle \quad (p=1),\\
|\psi_{1;[0,0]}\rangle &= |0_2^{\mathcal{E}}\rangle|0_1^{\mathcal{E}}\rangle|1^{\mathcal{S}}\rangle \quad (p=1),\\
|\psi_{0;[1,0]}\rangle &= |0_2^{\mathcal{E}}\rangle|1_1^{\mathcal{E}}\rangle|0^{\mathcal{S}}\rangle \quad (p=2),\\
&\vdots\\
|\psi_{1;[1,1]}\rangle &= |1_2^{\mathcal{E}}\rangle|1_1^{\mathcal{E}}\rangle|1^{\mathcal{S}}\rangle \quad (p=4).
\end{aligned} \tag{A2}$$

2. Equation of motion

The quantum Liouville equation is the equation of motion for the density matrix $\hat{\rho}(t)$ of the system-environment composite

$$\hat{\rho}(t) = e^{-\frac{i}{\hbar}\hat{H}t}\hat{\rho}(0)e^{+\frac{i}{\hbar}\hat{H}t}. \tag{A3}$$

3. Initial condition

As a next step, we establish the initial condition. The most general initial coherence vector $\vec{\lambda}^{\mathcal{S}}(0)$ is chosen for the system

$$\vec{\lambda}^{\mathcal{S}}(0) = [\lambda_1^{\mathcal{S}}(0), \lambda_2^{\mathcal{S}}(0), \lambda_3^{\mathcal{S}}(0)], \tag{A4}$$

and depolarized coherence vectors are chosen for environmental cells 1 and 2

$$\begin{aligned}
\vec{\lambda}^{\mathcal{E},1}(0) &= [\lambda_1^{\mathcal{E},1}(0), \lambda_2^{\mathcal{E},1}(0), 0],\\
\vec{\lambda}^{\mathcal{E},2}(0) &= [\lambda_1^{\mathcal{E},2}(0), \lambda_2^{\mathcal{E},2}(0), 0].
\end{aligned} \tag{A5}$$

The corresponding initial cellular density matrices $\hat{\rho}^{\mathcal{S}}(0)$, $\hat{\rho}^{\mathcal{E},1}(0)$, and $\hat{\rho}^{\mathcal{E},2}(0)$ may be constructed from the coherence vectors $\vec{\lambda}^{\mathcal{S}}(0), \vec{\lambda}^{\mathcal{E},1}(0)$, $\vec{\lambda}^{\mathcal{E},2}(0)$, and a symbolic form of the initial density matrix $\hat{\rho}(0)$ for the system-environment composite is obtained by taking the following direct product

$$\hat{\rho}(0) = \hat{\rho}^{\mathcal{E},2}(0) \otimes \hat{\rho}^{\mathcal{E},1}(0) \otimes \hat{\rho}^{\mathcal{S}}(0). \tag{A6}$$

In the derivation of an algebraic result, one must be careful with the mechanics: the order of the direct product must be consistent with the ordered basis B, and this order must be kept in mind when constructing the Hamiltonian $\hat{H}$.

4. Hamiltonian

Next, we construct the Hamiltonian matrix $\hat{H}$ in the B representation. The different dynamics between the system-environment-interaction-dominated case ($\chi \to \infty$) and the system-internal-dynamic-dominated case ($\chi \to 0$) demands a different $\hat{H}$ for each case. In both cases, however, our Hamiltonian is an 8×8 matrix, with rows and columns each corresponding to a unique $m_0; \vec{m}_p$ pairing

$$\begin{aligned}
&\text{Row or Column } 1 \leftrightarrow m_0 = 0;\ \vec{m}_p = [0,0],\\
&\text{Row or Column } 2 \leftrightarrow m_0 = 1;\ \vec{m}_p = [0,0],\\
&\text{Row or Column } 3 \leftrightarrow m_0 = 0;\ \vec{m}_p = [1,0],\\
&\qquad\vdots\\
&\text{Row or Column } 8 \leftrightarrow m_0 = 1;\ \vec{m}_p = [1,1].
\end{aligned} \tag{A7}$$

5. System-environment interaction dominates system internal dynamics

We implement the case where system-environment interaction dominates by setting $\gamma_{\mathcal{S}} = 0$. This disables switching by inter-dot tunneling in the system cell; and by design, switching is prohibited in environmental cells. Thus, there is no coupling between basis states in the evolution of this system-environment composite, and all off-diagonal terms of $\hat{H}$ are zero. The diagonal terms, however, are nontrivial, and they correspond to electrostatic potential energy of the array of molecules—both system and environmental—in the states as given by the subscripting label $m_0; \vec{m}_p$ of each diagonal term. Thus, the Hamiltonian in the B representation takes the diagonal form

$$\hat{H} = \begin{bmatrix} E_{0;[0,0]} & & & \\ & E_{1;[0,0]} & & \\ & & \ddots & \\ & & & E_{1;[1,1]} \end{bmatrix}. \tag{A8}$$

Next, we calculate the full density matrix $\hat{\rho}(t)$ for the system-environment composite using Eq. (A3) with the symbolic forms $\hat{H}$ and $\hat{\rho}(0)$ in Eqs. (A8) and (A6), respectively.

Then, we calculate the system cell's reduced density matrix $\hat{\rho}^r_{\mathcal{S}}(t)$ by summing over the $N_{\mathcal{E}}$ degrees of freedom $\vec{m}_p$ of the environment

$$[\hat{\rho}^r_{\mathcal{S}}(t)]_{m_o,m'_o} = \sum_{p=1}^{N_{\mathcal{E}}} [\hat{\rho}(t)]_{p,p,m_0,m'_0}. \tag{A9}$$

More explicitly, $\hat{\rho}^r_{\mathcal{S}}(t)$ is found element-wise from the elements of $\hat{\rho}(t)$:

$$\begin{aligned}
[\hat{\rho}^r_{\mathcal{S}}(t)]_{1,1} &= [\hat{\rho}(t)]_{1,1} + [\hat{\rho}(t)]_{3,3} + [\hat{\rho}(t)]_{5,5} + [\hat{\rho}(t)]_{7,7},\\
[\hat{\rho}^r_{\mathcal{S}}(t)]_{1,2} &= [\hat{\rho}(t)]_{1,2} + [\hat{\rho}(t)]_{3,4} + [\hat{\rho}(t)]_{5,6} + [\hat{\rho}(t)]_{7,8},\\
[\hat{\rho}^r_{\mathcal{S}}(t)]_{2,1} &= [\hat{\rho}(t)]_{2,1} + [\hat{\rho}(t)]_{4,3} + [\hat{\rho}(t)]_{6,5} + [\hat{\rho}(t)]_{8,7},\\
[\hat{\rho}^r_{\mathcal{S}}(t)]_{2,2} &= [\hat{\rho}(t)]_{2,2} + [\hat{\rho}(t)]_{4,4} + [\hat{\rho}(t)]_{6,6} + [\hat{\rho}(t)]_{8,8}.
\end{aligned} \tag{A10}$$

Here, counting number indices are used for element subscripting.

Finally, we calculate the components of the coherence vector using the elements of the system cell's reduced density matrix

$$\begin{aligned}
\lambda^{\mathcal{S}}_1(t) &= [\hat{\rho}^r_{\mathcal{S}}(t)]_{2,1} + [\hat{\rho}^r_{\mathcal{S}}(t)]_{1,2},\\
\lambda^{\mathcal{S}}_2(t) &= \frac{[\hat{\rho}^r_{\mathcal{S}}(t)]_{2,1} - [\hat{\rho}^r_{\mathcal{S}}(t)]_{1,2}}{i},\\
\lambda^{\mathcal{S}}_3(t) &= [\hat{\rho}^r_{\mathcal{S}}(t)]_{1,1} - [\hat{\rho}^r_{\mathcal{S}}(t)]_{2,2}.
\end{aligned} \tag{A11}$$

Direct algebraic analysis of Mathematica® output from code implementing Eqs. (A3)–(A11) yields an expression in terms of the differences $E_{1;\vec{m}_p} - E_{0;\vec{m}_p}$. We recognize this as the energy $E^{\text{flip}}_{\vec{m}_p}$ required to flip the system bit from "0" to "1" while the environment maintains the state given by $\vec{m}_p$

$$E^{\text{flip}}_{\vec{m}_p} \equiv E_{1;\vec{m}_p} - E_{0;\vec{m}_p}. \tag{A12}$$

Thus, our algebraic result for the components of system cell's time evolution when system-environment interaction dominates system internal dynamics is

$$\begin{aligned}
\lambda^{\mathcal{S}}_1(t) &= \lambda^{\mathcal{S}}_1(0) f(t),\\
\lambda^{\mathcal{S}}_2(t) &= \lambda^{\mathcal{S}}_2(0) f(t), \quad \text{and}\\
\lambda^{\mathcal{S}}_3(t) &= \lambda^{\mathcal{S}}_3(0),
\end{aligned} \tag{A13}$$

where

$$f(t) = \frac{1}{N_{\mathcal{E}}} \sum_{p=1}^{N_{\mathcal{E}}} \cos\left(\frac{E^{\text{flip}}_{\vec{m}_p}}{\hbar} t\right). \tag{A14}$$

6. System internal dynamics competes with system-environment interaction

Now we repeat our analysis, which differs from the case given in Section A.5 by the construction of the Hamiltonian $\hat{H}$. Previously, we set the system cell's tunneling energy $\gamma_{\mathcal{S}}$ to zero to allow system-environment interaction to dominate system internal dynamics in driving overall dynamics. Now, we have a finite $\gamma_{\mathcal{S}}$, and this manifests itself in coupling composite states with the same environmental state, but different system states. This results in a Hamiltonian with the form

$$\hat{H} = \begin{bmatrix}
E_{0;[0,0]} & -\gamma_{\mathcal{S}} & & & & \\
-\gamma_{\mathcal{S}} & E_{1;[0,0]} & & & & \\
 & & \ddots & & & \\
 & & & E_{0;[1,1]} & -\gamma_{\mathcal{S}} & \\
 & & & -\gamma_{\mathcal{S}} & E_{1;[1,1]}
\end{bmatrix}. \tag{A15}$$

With the Hamiltonian in this form, we implement Eqs. (A3)–(A11) with Eq. (A15) in lieu of Eq. (A8) in Mathematica® and simplify the output corresponding to Eq. (A11) by direct algebraic analysis to yield

$$\begin{aligned}
\lambda^{\mathcal{S}}_1(t) &= \frac{\lambda^{\mathcal{S}}_1(0)}{N_{\mathcal{E}}} \sum_{p=1}^{N_{\mathcal{E}}} \frac{4\gamma^2_{\mathcal{S}} + (E^{\text{flip}}_{\vec{m}_p})^2 \cos\left(\frac{\epsilon_{\vec{m}_p}}{\hbar} t\right)}{\epsilon^2_{\vec{m}_p}},\\
\lambda^{\mathcal{S}}_2(t) &= \frac{\lambda^{\mathcal{S}}_2(0)}{N_{\mathcal{E}}} \sum_{p=1}^{N_{\mathcal{E}}} \cos\left(\frac{\epsilon_{\vec{m}_p}}{\hbar} t\right) + \cdots\\
&\quad + \frac{\lambda^{\mathcal{S}}_3(0)}{N_{\mathcal{E}}} \sum_{p=1}^{N_{\mathcal{E}}} \frac{2\gamma_{\mathcal{S}}}{\epsilon_{\vec{m}_p}} \sin\left(\frac{\epsilon_{\vec{m}_p}}{\hbar} t\right), \text{ and}\\
\lambda^{\mathcal{S}}_3(t) &= -\frac{\lambda^{\mathcal{S}}_2(0)}{N_{\mathcal{E}}} \sum_{p=1}^{N_{\mathcal{E}}} \frac{2\gamma_{\mathcal{S}}}{\epsilon_{\vec{m}_p}} \sin\left(\frac{\epsilon_{\vec{m}_p}}{\hbar} t\right) + \cdots\\
&\quad + \frac{\lambda^{\mathcal{S}}_3(0)}{N_{\mathcal{E}}} \sum_{p=1}^{N_{\mathcal{E}}} \frac{4\gamma^2_{\mathcal{S}} \cos\left(\frac{\epsilon_{\vec{m}_p}}{\hbar} t\right) + (E^{\text{flip}}_{\vec{m}_p})^2}{\epsilon^2_{\vec{m}_p}},
\end{aligned} \tag{A16}$$

where

$$\epsilon_{\vec{m}_p} = \sqrt{4\gamma^2_{\mathcal{S}} + (E^{\text{flip}}_{\vec{m}_p})^2}. \tag{A17}$$

Equations (A16) and (A17) are a more general case of Eq. (A13), which may be obtained from Eqs. (A16) and (A17) in the limit of small $\gamma_{\mathcal{S}}$.

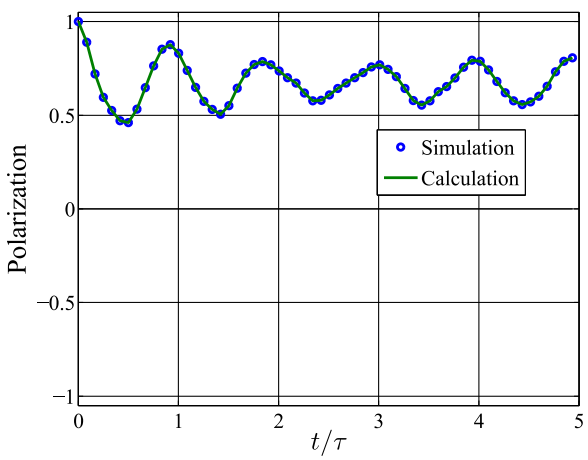

FIG. 23. Exact agreement between calculated polarization and simulated polarization for a target cell in an eight-cell environment. We used Eq. (A16) to calculate the evolution of the system cell's coherence vector (green line). This matches perfectly with the polarization obtained from full simulation of the system-environment composite (blue circles).

7. Calculations using Eq. (A16)

Now we show, the accuracy of Eq. (A16) in Figure 23, which provides a comparison between the results of the full coherent simulation of the system-environment composite and the calculated results using this equation. The agreement is exact.

Figure 15, which provides a polarization trace for a system cell interacting with an 26-cell environment ($N = 26$), is a demonstration of the power of this equation. A full simulation of this size would require 262, 144 TB of memory to store $\hat{\rho}(t)$ alone, but a calculation of $\vec{\lambda}^{S}(t)$ based on Eq. (A16) is quite feasible.

[1]K. Galatsis, A. Khitun, R. Ostroumov, K. L. Wang, W. R. Dichtel, E. Plummer, J. F. Stoddart, J. I. Zink, J. Y. Lee, Y.-H. Xie, and K. W. Kim, "Alternate state variables for emerging nanoelectronic devices," IEEE Trans. Nanotechnol. **8**, 66 (2009).

[2]J. J. Welser, G. I. Bourianoff, V. V. Zhirnov, and R. K. Cavin, "The quest for the next information processing technology," J. Nanopart. Res. **10**, 1 (2008).

[3]C. S. Lent and P. D. Tougaw, "A device architecture for computing with quantum dots," Proc. IEEE **85**, 541–557 (1997).

[4]C. S. Lent and B. Isaksen, "Clocked molecular quantum-dot cellular automata," IEEE Trans. Electron Devices **50**, 1890–1896 (2003).

[5]M. T. Niemier, M. J. Kontz, and P. M. Kogge, "A design of and design tools for a novel quantum dot based microprocessor," in *37TH Design Automation Conference Proceedings*, (2000), pp. 227–232.

[6]S. Gardelis, C. G. Smith, J. Cooper, D. A. Ritchie, E. H. Linfield, and Y. Jin, "Evidence for transfer of polarization in a quantum dot cellular automata cell consisting of semiconductor quantum dots," Phys. Rev. B **67**, 033302 (2003).

[7]M. Mitic, M. C. Cassidy, K. D. Petersson, R. P. Starrett, E. Gauja, R. Brenner, R. G. Clark, A. S. Dzurak, C. Yang, and D. N. Jamieson, "Demonstration of a silicon-based quantum cellular automata cell," Appl. Phys. Lett. **89**, 013503 (2006).

[8]M. B. Haider, J. L. Pitters, G. A. DiLabio, L. Livadaru, J. Y. Mutus, and R. A. Wolkow, "Controlled coupling and occupation of silicon atomic quantum dots at room temperature," Phys. Rev. Lett. **102**, 046805 (2009).

[9]G. H. Bernstein, A. Imre, V. Metlushko, A. Orlov, L. Zhou, L. Ji, G. Csaba, and W. Porod, "Magnetic QCA systems," Microelectron. J. **36**, 619–624 (2005).

[10]M. Taucer, F. Karim, K. Walus, and R. A. Wolkow, "Consequences of many-cell correlations in treating clocked quantum-dot cellular automata circuits," e-print arXiv:1207.7008 [cond-mat.mes-hall].

[11]W. H. Zurek, "Decoherence, einselection, and the quantum origins of the classical," Rev. Mod. Phys. **75**, 715–775 (2003).

[12]A. Ben-Naim, *A Fairwell to Entropy: Statistical Mechanics Based on Information* (World Scientific, 2008).

[13]Y. Lu and C. Lent, "Self-doping of molecular quantum-dot cellular automata: Mixed valence zwitterions," Phys. Chem. Chem. Phys. **13**, 14928–14936 (2011).

[14]H. Qi, S. Sharma, Z. H. Li, G. L. Snider, A. O. Orlov, C. S. Lent, and T. P. Fehlner, "Molecular quantum cellular automata cells. Electric field driven switching of a silicon surface bound array of vertically oriented two-dot molecular quantum cellular automata," J. Am. Chem. Soc. **125**, 15250–15259 (2003).

[15]H. Qi, A. Gupta, B. C. Noll, G. L. Snider, Y. H. Lu, C. Lent, and T. P. Fehlner, "Dependence of field switched ordered arrays of dinuclear mixed-valence complexes on the distance between the redox centers and the size of the counterions," J. Am. Chem. Soc. **127**, 15218–15227 (2005).

[16]G. Mahler and V. A. Weberruss, *Quantum Networks: Dynamics of Open Nanostructures* (Springer, 1995).

[17]E. T. Jaynes, *Probability Theory: The Logic of Science* (Cambridge University Press, 2003).

[18]C. E. Shannon and W. Weaver, *The Mathematical Theory of Communication* (University of Illinois Press, 1998).

[19]B. Schumacher and M. Westmoreland, *Quantum Processes Systems, and Information* (Cambridge University Press, 2010).

[20]E. P. Blair, M. Liu, and C. S. Lent, "Signal energy in quantum-dot cellular automata bit packets," J. Comput. Theor. Nanosci. **8**, 972–982 (2011).

[21]J. Timler and C. S. Lent, "Maxwell's demon and quantum-dot cellular automata," J. Appl. Phys. **94**, 1050–1060 (2003).

[22]P. D. Tougaw and C. S. Lent, "Dynamic behavior of quantum cellular automata," J. Appl. Phys. **80**, 4722–4736 (1996).

[23]G. Toth and C. S. Lent, "Role of correlation in the operation of quantum-dot cellular automata," J. Appl. Phys. **89**, 7943–7953 (2001).